UNSTEADY AERODYNAMICS &TURBULENT NEAR-WAKE CHARACTERIZATION OF

STATIC & ROTATING CYLINDER SYSTEMS

A Thesis
Submitted to the Graduate Faculty
of the
North Dakota State University
of Agriculture and Applied Science

By

Braden Lee Rostad

In Partial Fulfillment of the Requirements
for the Degree of
MASTER OF SCIENCE

Major Department:
Mechanical Engineering

April 2018

Fargo, North Dakota

North Dakota State University
Graduate School

Title

Unsteady Aerodynamics and Turbulent Near-Wake Characterization of
Static and Rotating Cylinder Sytems

By

Braden Lee Rostad

The Supervisory Committee certifies that this ***disquisition*** complies with North Dakota

State University's regulations and meets the accepted standards for the degree of

MASTER OF SCIENCE

SUPERVISORY COMMITTEE:

Dr. Jordi Estevadeordal

Chair

Dr. Bora Suzen

Dr. Yan Zhang

Dr. Mark Strand

Approved:

4/13/2018	Dr. Alan R. Kallmeyer
Date	Department Chair

ABSTRACT

External flows around bluff bodies have been broadly investigated due to their great importance in engineering applications including aircraft and missile development, marine and naval structures, vehicle aerodynamics, wind power generation, and turbulence near suspension bridge cables. The circular cylinder has been the topic of a significant portion of this research due to its simple geometry and its ability to generally represent numerous engineered and natural structures. The goal of Phase 1 of this is to capture and analyze wake structures formed by variations on the geometry of a circular cylinder. The goal of Phase 2 is to observe the effects of artificially generated turbulence on the flow over a dimpled airfoil. High-image-density particle image velocimetry (PIV) is used to obtain velocity vector fields, flow standard deviation, and vorticity.

ACKNOWLEDGEMENTS

DEDICATION

To my son, Edison, may your curiosity lead you down interesting paths.

-Dad

TABLE OF CONTENTS

LIST OF TABLES

LIST OF FIGURES

LIST OF SYMBOLS

Re ....Reynolds number, $\frac{\rho v L_{ref}}{\mu}$

ρ ....Fluid density, kg/m^3

v ....Flow velocity, m/s

μ ....Dynamic viscosity, $N \cdot s/m^2$

L_{ref} ....Reference length, m

T ....Temperature, ℃

υ ....Kinematic viscosity, m^2/s

δ ....Boundary layer height, m

u ....x component of velocity, m/s

v ....y component of velocity, m/s

w ....z component of velocity, m/s

$|V|$ ....Velocity magnitude, m/s

g ....Gravitational acceleration, m/s^2

M ....Mach number

s...Displacement, m

t ....Time, s

σ ....Standard deviation

1. INTRODUCTION

Both the near and far wake structures behind a bluff body in fluid flow have been topics of extensive research. Using numerical approaches, computational fluid dynamics (CFD), and particle image velocimetry (PIV); researchers have attempted to characterize or control the flow and separation points behind various geometries. One primary goal of existing research has been to delay the flow separation from the surface of the body. The first known attempt to investigate the effects of a rotating cylinder in fluid flow were made by German physicist Heinrich Gustav Magnus who proved that a rotating cylinder in a flow caused a difference in pressure above and below the cylinder resulting in lift called the 'Magnus Effect' [6]. The area of interest in the present study is the flow structures in the near wake of static and rotating cylinder geometries. There is no prescription for the term near wake however it was defined by [18] as the region up to ten diameters downstream from the cylinder. The aim of this study is to compare experimental results obtained from static and rotating bluff bodies in fluid flow. Bluff bodies are defined as a body that, as a result of its shape, has separated flow over a substantial part of its surface. An important feature of a bluff body flow is that there is a very strong interaction between the viscous and inviscid regions. Cylinders and spheres are considered bluff bodies because at large Reynolds numbers the drag is dominated by the pressure losses in the wake. In this investigation the turbulent wakes formed by a circular cylinder (Fig. 1.1), sliced cylinder (Fig. 1.2), and a three-cylinder arrangement (Fig. 1.3) will be observed and analyzed. Flow data will be taken with the cylinder systems in both a static and rotating condition. To further study the effects of turbulent wakes, a dimpled airfoil will be placed behind the rotating three-cylinder system to observe the effects of artificially generated turbulence on flow separation. This investigation aims to accomplish the following using two-dimensional velocity vector fields; (i) Observe the effects of rotation speeds on the formation

1

of the vortex street turbulence (ii) Quantify the effects of Reynolds number on the near wake vortex

structure (iii) Observe the effects of the bluff body on an airfoil downstream of the body.
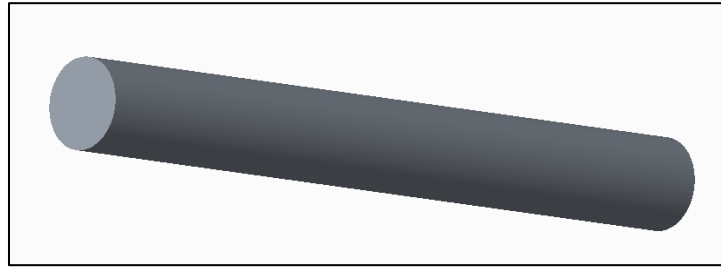

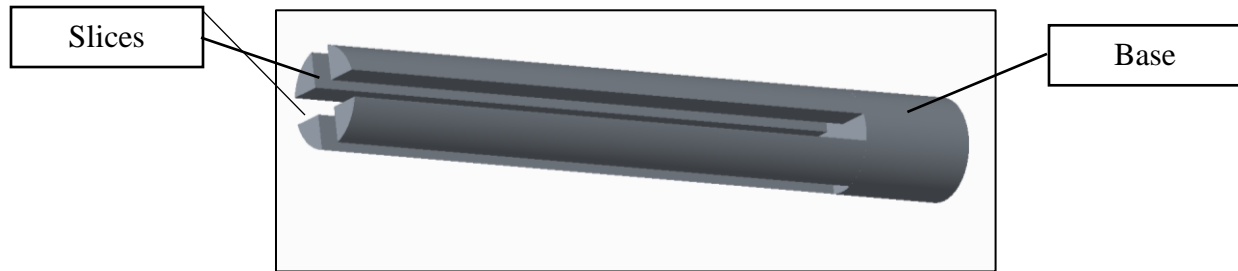Fig. 1.1. Circular cylinder ($diameter = 2.54cm\ length = 23.0cm$)

Fig. 1.2. Sliced cylinder ($diameter = 2.54cm\ length = 23.0cm\ slit\ width = .67cm$)
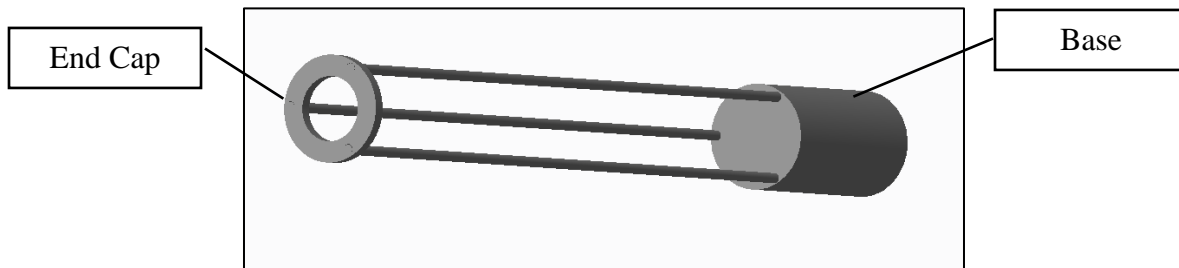
Fig. 1.3. Three-cylinder arrangement ($diameter = 0.24cm\ length = 23.0cm$)

2. FUNDAMENTAL CONCEPTS

2.1. Flow Properties

Flow about a bluff body must be examined with close attention paid to several fluid properties. To begin our understanding of the turbulence created by a circular cylinder in a flow we must first understand how various fluid properties will affect the pressure, kinetic energy, and Reynolds number. To start, we will assume that the fluid is continuous and incompressible. Flow velocities for this experiment will range from $0.05\ to\ 17.3\ m/s$ and the air in the wind tunnel will be at standard atmospheric conditions where the maximum Mach number will be $M = 0.05$ making this an incompressible flow.

Another important dimensionless number for this study is Reynold's number. The Reynold's number is used to predict the flow behavior of various conditions tested in this study. The Reynold's number is the ratio of viscous to inertial forces in a flow. For high Reynolds numbers it is known that the viscous forces will dominate the flow and conversely for low Reynolds numbers the inertial forces will dominate. Reynolds number is characterized by the following quantities;

$$Re = \frac{\rho u L}{\mu} = \frac{uL}{v} \qquad\qquad \text{(Eq. 2.1)}$$

Three different cylinder geometries have been examined in this study. All three geometries were tested in a static (non-rotating) and rotating condition. Rotation speed was controlled by a DC power supply connected to a motor and driveshaft. More on the construction and setup of the cylinder mount assembly can be found in the "Experimental Methodology" section. The profiles of the bluff bodies have been named as follows; full circular cylinder, sliced cylinder, and three-cylinder arrangement as seen in Figs. 2.1 thru Fig. 2.3.

Fig. 2.1. Raw Image: Circular cylinder
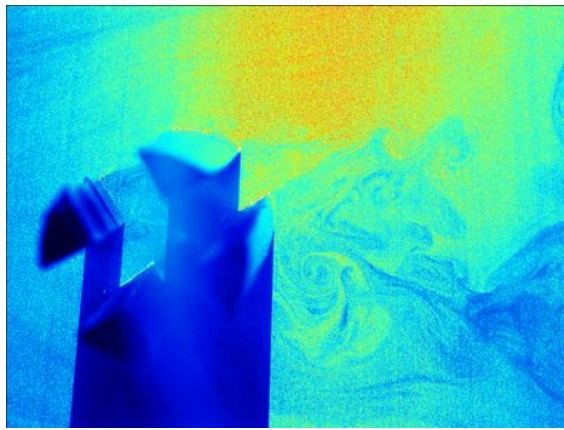
Fig. 2.2. Raw Image: Sliced cylinder

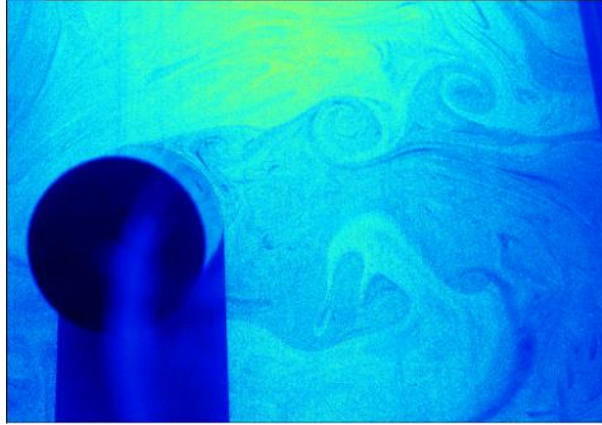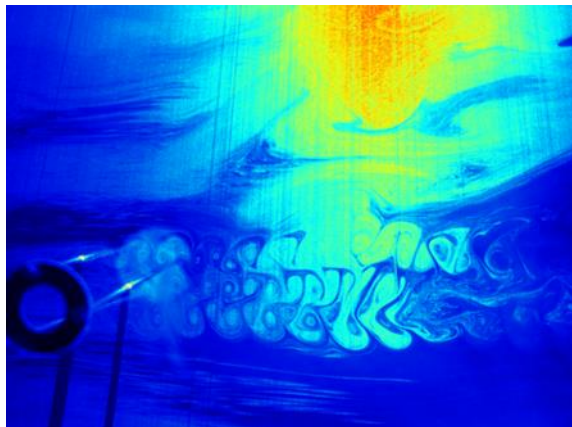Fig. 2.3. Raw Image: Three-cylinder arrangement

Reynolds numbers for each body geometry were calculated using the following characteristic lengths; circular cylinder $L = 2.54cm$ (diameter), sliced cylinder $L = 2.54cm$ (diameter), three-cylinder arrangement, $L = 0.24cm$ (diameter). Air at atmospheric conditions and room temperature was used as the test fluid. Specific properties of the operating fluid are as follows; temperature $T = 22°C$, dynamic viscosity $v = 18.23 \times 10^{-6} \, Pa \cdot s$. Based upon these conditions the Reynolds numbers dealt with in this investigation are as follows;

Table 2.1. Reynolds numbers

Reynolds Numbers For All Conditions				
Windtunnel fan Input (%)	Free Stream Velocity (m/s)	Circular Cylinder (L=2.54cm)	Sliced Cylinder (L=2.54cm)	Three Cylinder Arrangement (L=.24cm)
1	**0.05**	83	83	8
3	**0.1**	166	166	16
5	**0.2**	333	333	31
10	**4.1**	6824	6824	645
20	**9.25**	15396	15396	1455
30	**12.3**	20473	20473	1934
40	**17.3**	28796	28796	2721

Note: This table lists Reynolds numbers used in the present study for all cylinder profiles.

2.2. Equations Governing the Flow

For this study we will consider the flow to be three-dimensional and incompressible since the Mach number is less than 0.3. The governing equations for this type of flow are obtained from manipulation of the Navier-Stokes equations. These equations account for pressure forces, body forces, surface forces, and viscous forces and can be written as follows;

$$\frac{\partial u}{\partial x} + \frac{\partial u}{\partial y} + \frac{\partial u}{\partial z} = 0 \qquad \text{(Eq. 2.2)}$$

$$\rho\left(\frac{\partial u}{\partial t} + u\frac{\partial u}{\partial x} + v\frac{\partial u}{\partial y} + w\frac{\partial u}{\partial z}\right) = -\frac{\partial p}{\partial x} + \mu\left(\frac{\partial^2 u}{\partial x^2} + \frac{\partial^2 u}{\partial y^2} + \frac{\partial^2 u}{\partial z^2}\right) + \rho g_x \quad \text{(Eq. 2.3)}$$

$$\rho\left(\frac{\partial v}{\partial t} + u\frac{\partial v}{\partial x} + v\frac{\partial v}{\partial y} + w\frac{\partial v}{\partial z}\right) = -\frac{\partial p}{\partial y} + \mu\left(\frac{\partial^2 v}{\partial x^2} + \frac{\partial^2 v}{\partial y^2} + \frac{\partial^2 v}{\partial z^2}\right) + \rho g_y \quad \text{(Eq. 2.4)}$$

$$\rho\left(\frac{\partial w}{\partial t} + u\frac{\partial w}{\partial x} + v\frac{\partial w}{\partial y} + w\frac{\partial w}{\partial z}\right) = -\frac{\partial p}{\partial z} + \mu\left(\frac{\partial^2 w}{\partial x^2} + \frac{\partial^2 w}{\partial y^2} + \frac{\partial^2 w}{\partial z^2}\right) + \rho g_z \quad \text{(Eq. 2.5)}$$

This investigation made use of a two-dimensional particle image velocimetry flow visualization technique. However, the flow is described most accurately by the three-dimensional Navier-Stokes equations. To obtain the best results of a three-dimensional flow, a tomographic study would be required.

2.3. Boundary Layer Formation

2.3.1. Flat Plate

The study of any body in a viscous flow must include a discussion of boundary layer formation. The two shapes most commonly observed with regard to boundary layer formation are that of the flat plate, and the circular cylinder. One of the first scientists to study the boundary layer was Ludwig Prandtl. He observed that the influence of viscosity was confined to a very thin layer in the immediate neighborhood of the solid boundary. In this thin layer called the boundary layer the frictional forces retarded the motion of the fluid. As the fluid continued to move along the solid boundary, the boundary layer would increase in height [23]. Boundary layer thickness is somewhat subjective since the velocity in the boundary layer asymptotically approaches the free stream velocity. Owing to this, it has been generally accepted that the perpendicular distance from the wall to the location where the free stream and boundary layer velocity differ by 1% is the height of the boundary layer. The equation for boundary layer thickness, δ, can be written as follows;

$$\delta = \int_{0}^{\infty} (U - \boldsymbol{u})dy \qquad \text{(Eq. 2.6)}$$

As the flow moves along the flat plate, Prandtl noted that the boundary layer would continue to grow and intermittently develop small swirling vortexes along with a still mostly laminar flow. This section of the boundary layer is known as the transitional region. Further still along the flat plate, the swirling vortexes would grow in size and number eventually dominating the flow. This final region is known as the turbulent region [6]. All three regions can be seen in Fig. 2.4.
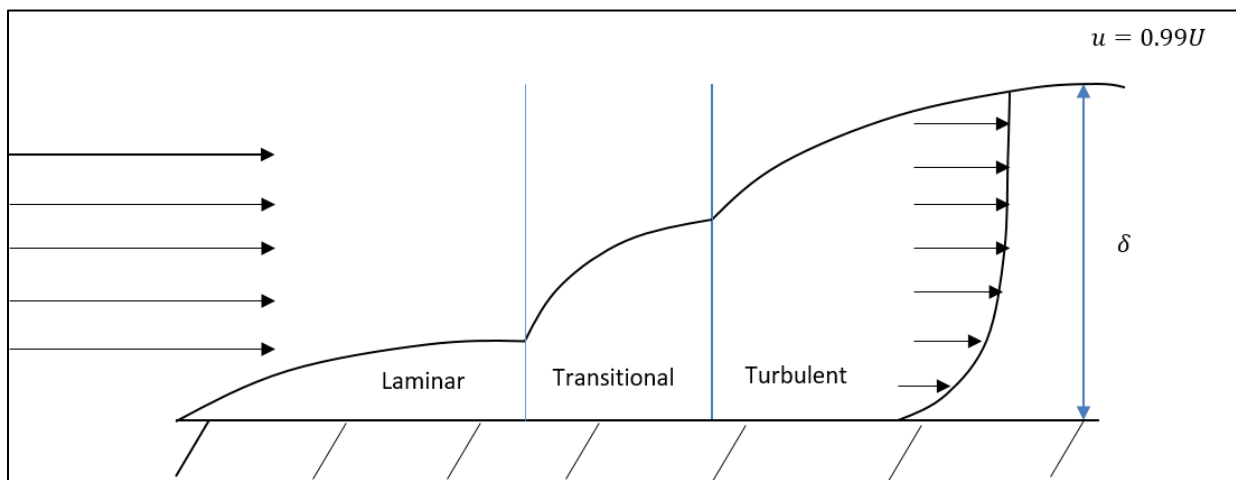
Fig. 2.4. Boundary layer over flat plate adapted from [6]

The phenomena of laminar, to transitional, to turbulent flow is caused by an increased thickness of the boundary layer leading to pressure differences in the flow where the static pressure of the environment remains constant. It may also be characterized by the dimensionless Reynold's number where it has been shown experimentally that various ranges of Reynold's numbers correspond to varying flow behavior as follows;

Table 2.2. Flow conditions

Flow Condition	Reynolds Number
Laminar	<2300
Transitional	2300-4000
Turbulent	>4000

Note: Flow conditions and Reynolds Numbers adapted from [7]

In the turbulent area a pressure difference causes reversal in the flow leading to the deceleration of fluid particles forcing them outward. The flow of fluid across a flat plate is a relatively simple case which highlights the basic phenomena in the boundary layer [23].

2.3.2. Circular Cylinder

Now that boundary layer formation on a flat plate has been addressed, we can look at boundary layer formation around a circular cylinder. Boundary layer separation is strongly associated with the flow around bluff bodies where immediately behind the body there exists a region of greatly decelerated flow or "wake". The present study will concentrate on the type of flow where the wake region is characterized by a significant pressure gradient. The development of a steep pressure gradient is most obvious in the case of a circular cylinder. In contrast to the case of a flat plate, where atmospheric pressure is impressed upon the flow, a low-pressure area develops behind the cylinder. The low-pressure area then causes an adverse pressure gradient and backflow. The change in the boundary layer and resulting backflow can be seen in Fig. 2.5.
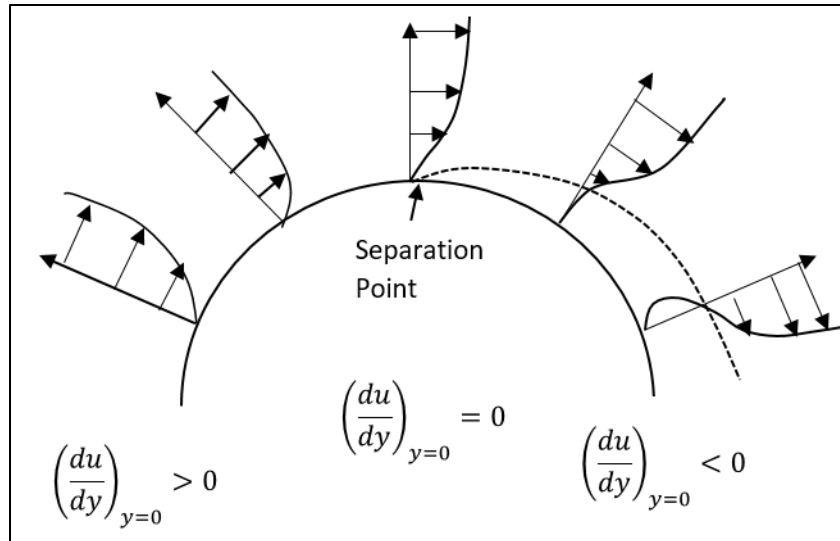
Fig. 2.5. Boundary layer over circular cylinder adapted from [6]

If we imagine a fluid particle travelling toward the center of the cylinder it will first experience a total loss in kinetic energy at the stagnation point. The particle will then be deflected around the cylinder where its kinetic energy rapidly increases until it is at the top of the cylinder. At this point, the particle will again lose kinetic energy due to the adverse pressure gradient until it reverses direction. The point at which the bottom layer of particles has reversed direction is called the separation point [23]. From this point on the flow has been separated from the boundary and turbulent wake results.

At low Reynolds numbers the near wake of a cylinder is characterized by unseparated flow or a fixed pair of counter rotating vortices as seen in Fig. 2.6 a) and b). As the Reynolds number increases we begin to see counter rotating vortices shed on alternating sides of the body. Finally, at $Re > 3 \times 10^5$ we begin to get completely turbulent flow followed by the re-establishment of a turbulent vortex street as seen in Fig. 2.6 c) through e).
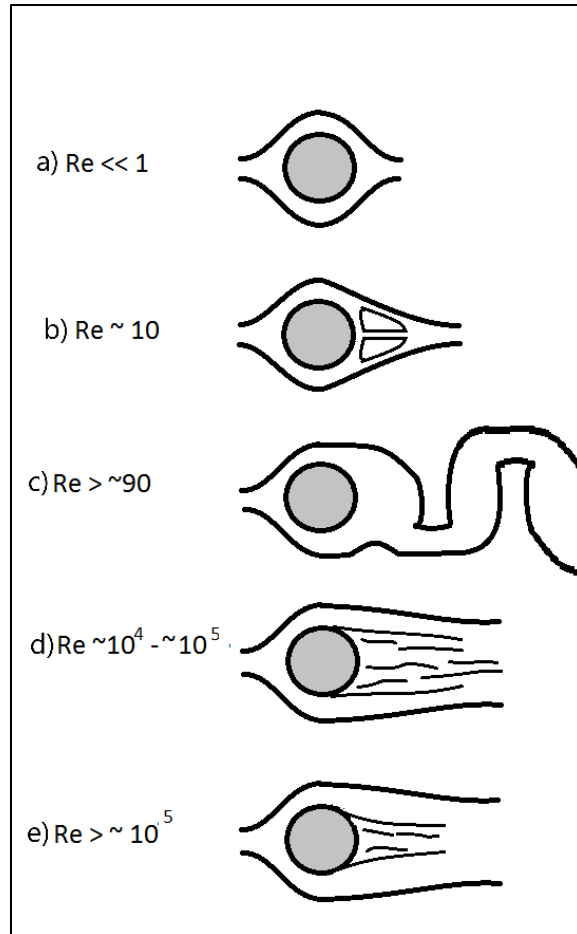
9

Fig. 2.6. Effect of Reynolds number on wake patterns [29]

3. PREVIOUS WORK

Experimental and numerical results for flow past a single circular cylinder is of great importance in the study of fluid flow. In the laminar region, it has been shown that a stable wake flow with a single vortex pair begins near $Re = 6.2$ [4], [24].

The next significant development in the wake flow begins at $Re > 47$ where alternate vortex shedding appears [20], [12], [3]. The next step in isolated, static cylinder flow is the formation of a repeating pattern of alternating swirling vortexes known as the von Karman vortex street. This phenomenon is typically observed at $Re > 90$ where it is two-dimensional until Re>170 [31]. It was then suggested that the two-dimensional Karman vortex street enters a "Mode A" instability near a critical Reynold's number of $Re = 188.5 \pm 1.0$ [9].

Numerical studies have been an important part cylinder wake study. An attempt was made by [2] to simulate the unsteady turbulent vortex structure downstream of a static cylinder using a Reynolds-Averaged Navier-Stokes CFD simulation. The study was performed to assess the capability of unstructured grids and large eddy simulations with no sub grid scale model for the three-dimensional flow. A Reynolds number of 20,000 was used in this investigation and it was found that the turbulence intensity as a function of distance from the trailing edge of the cylinder was in line with experimental PIV results obtained in by [15]. The authors of [18], using systematic spectral direct (DNS) and large-eddy simulation (LES) at Reynolds numbers between 500 and 5000, found that the very near wake, up to 3 cylinder diameters is dominated by shear layer dynamics and is very sensitive to disturbances in the cylinder aspect ratio. The researchers in [5] investigated the near wake of a cylinder at Reynolds numbers corresponding to the onset and development of shear-layer instabilities. This investigation compared a numerical simulation to experimental data and found that for varying Reynolds numbers the mean velocity, vorticity,

11

Reynolds stress, and r.m.s. fluctuations in the wake structure are notably altered. The variation of Reynolds number also influenced the shear-layer instability. The investigation revealed that at a lower turbulent Reynolds numbers the shear-layer velocity was characterized by high-frequency low-amplitude fluctuations caused by shear-layer vortices superimposed on top of large-scale fluctuations caused by the Karman vortex formation. At higher Reynolds numbers the fluctuations dominated the shear-layer velocity and overwhelmed the fluctuations caused by Karman vortex formation [5].

The wake structure behind a two-cylinder setup has also been well studied. The arrangements include cylinders in tandem, side by side, or staggered [12], [19], [26], [27], [14]. The most widely studied of the aforementioned arrangements are that of two cylinders in tandem. Reynold's numbers from 8.7×10^3 to 5.2×10^4 and center to center distance/diameter ratios from 1.03 to 5.0 have been used to examine the wake structures experimentally. In this arrangement, eight different flow regimens were discovered where the fluid forces were greatly dependent on Reynold's number [10]. A numerical study conducted at low Reynold's number (Re=100) for varying cylinder spacing in [25] suggested that there exists a critical separation distance between 3.75 and 4.0 diameters, where significant jumps in the alternating forces and Strouhal number occur. This suggests that in applications where cyclic loading forces are to be minimized, the primary consideration should be to avoid this critical spacing zone.

Investigations of side by side arrangements of circular cylinders have also yielded a significant amount of experimental results. In this arrangement, the general observations have been that vortex shedding occurs either in or out of phase depending on Reynolds number and cylinder spacing. In a numerical simulation at larger gap to diameter ratios, even at low Reynolds numbers ($1 \leq Re \leq 20$) it was shown by [30] that the flow patterns are significantly different from the case

of a single circular cylinder. They found that variations in lift coefficient caused by wake interference was a function of cylinder spacing. To describe the dynamic reactions of wake interference, a theoretical model was developed by [22] using the Landau equations combined with experimentally determined coefficients.

For the general case of two cylinders in a staggered arrangement [27] experimentally observed nine distinct flow patterns for 850<Re<1900. Later, using a numerical simulation [14] identified ten different patterns for flow in the laminar region. Next, experimental data was taken for varying stagger angles ($0\ to\ \pi$) and gap ratios ($0.1\ to\ 5.0$) by [1]. Using the variables of Strouhal number, fluid forces, and flow structure appearance, 19 distinct flow regimes were discovered.

The next layer of complexity in the study of cylinder arrangements is the addition of a third cylinder. Most studies of a three-cylinder system have been done using an equilateral arrangement where the cylinders are placed at the vertexes of an equilateral triangle. The researchers in [33] used a formation such as this with $60 < Re < 300$ to visually inspect the phenomena using smoke seeding. The authors of [14] also used an equilateral arrangement with small gap ratios to relate the analytical method of image doublets, which can be applied to an arbitrary number of cylinders, to the experimental data collected with three cylinders.

Effects of cylinder geometry and coating have also been studied experimentally. Using PIV, [11] analyzed the effect of applying a rough, hydrophobic, micro-textured coating on a cylinder in water flow to observe the turbulence transition and the formation of turbulent vortexes in the near wake. The texture applied to the cylinder was on the scale of $20\mu m$. It was found that the rough, hydrophobic surface directly affected the boundary layer at separation by reducing the size of the fluid recirculation bubble in the wake of the cylinder. It was also found that if the film

of air surrounding the cylinder was stably maintained, and if the gas fraction was large enough, that the subsequent turbulence enhancement around the cylinder would cause a delay in flow separation and facilitated early roll-up of the shed vortices. The conclusion was that by altering the surface roughness of the hydrophobic coating, one can passively control the flow and separation point of water around a static cylinder. Again, using PIV, the authors of [21] used a droplet shaped mesh around a cylinder in an attempt to passively control the flow. This showed that the interaction between the shear layers could be prevented with the mesh barrier. It resulted in the recirculating vortex in the cylinder wake being formed closer to the trailing edge. Another PIV experiment conducted by [8] used a circular cylinder with a slit cut out of the center to show that this eliminated the leading edge and trailing edge stagnation points at high Reynolds numbers. By eliminating the stagnation points, and allowing flow to pass through the cylinder, the vortex shedding frequency was greatly altered. Instead of a Karman vortex street, a pair of symmetric jet vortices were found to form in the near wake.

4. EXPERIMENTAL METHODOLOGY

4.1. PIV Setup

In the present study, experiments were conducted in a low speed open-circuit wind tunnel with an intake measuring $1.1m * 1.1m$ and a test section measuring $0.3m * 0.3m * 0.9m$. The wind tunnel is powered by a single axial fan with a diffuser radius of $0.7m$ and uses a system of honeycomb and wire mesh at the intake for flow damping. The cylinder models were installed $0.22m$ from the inlet of the test section and were affixed to a motor mount apparatus where the rotation speed was controlled by a DC power supply plugged into a standard 120V outlet. The motor mount apparatus was fashioned by welding rectangular aluminum tubing to form a stand and then attaching the motor to the inside of the tubing and the cylinder to the exterior as seen in Fig. 4.1. The drive shaft was connected to the cylinder through the wall of the aluminum tubing. Each cylinder profile could then be removed and exchanged. The Reynolds numbers for this investigation ranged from $8 - 28000$ based on cylinder diameter.
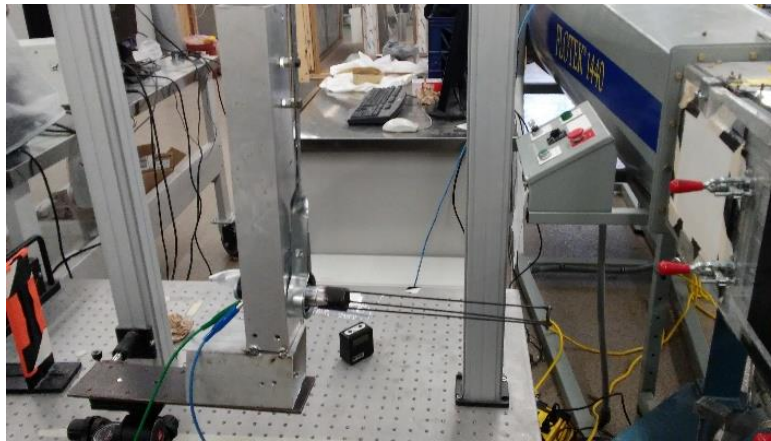

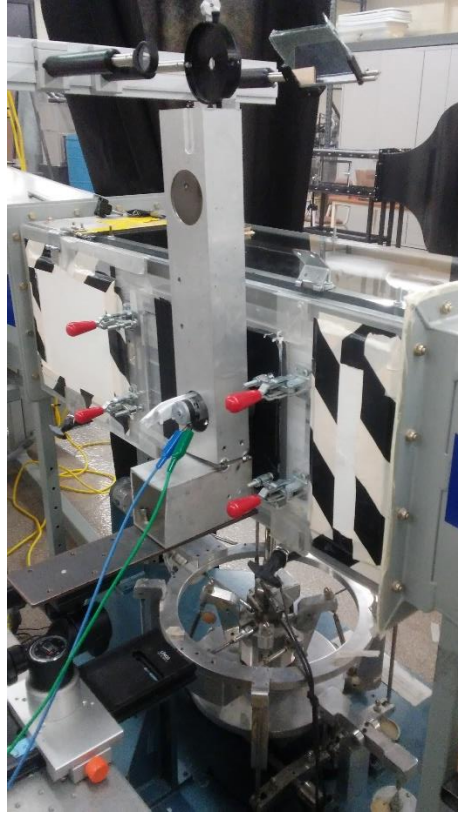Fig. 4.1. Three-cylinder system and motor mounting gear

Fig. 4.2. Cylinder system inserted into wind tunnel test section

PIV is an optical, experimental, flow visualization method which can be used to study flow velocities and wake structures in a wind tunnel setup. The PIV method relies on high speed cameras and lasers which are controlled by a timing unit. The cameras and lasers are synchronized to capture two images very close together (on the order of $50 - 500\mu s$). Cross correlation techniques are then used to determine the velocity vector field.
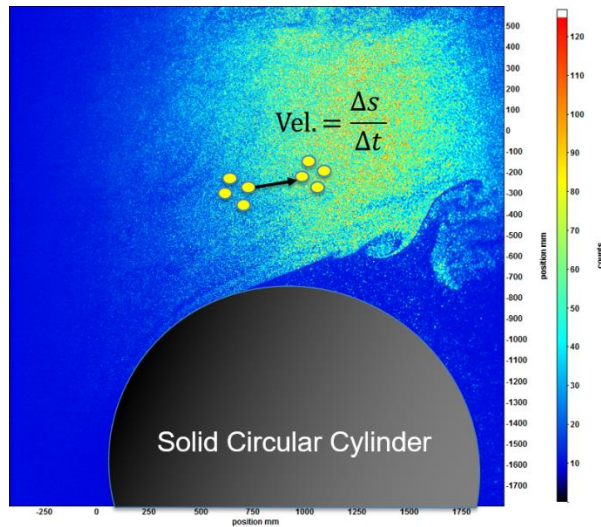
Fig. 4.3. Cross correlation representation

Illumination of the model was provided by a double-pulsed Nd:YAG laser (NewWave MiniLase-III) emitting two laser pulses of 100 mJ at a wavelength of 532 nm with a repetition rate of 15 Hz. The laser beam was shaped to a laser sheet (thickness $< 1\ mm$) by using a set of mirrors, spherical lenses, and cylindrical lenses. The illuminated test section can be seen in Fig. 4.4. The flow was seeded by Di-Ethyl-Hexyl-Sebacat (DEHS) oil droplets (LaVision GMbH) using a pressurized reservoir connected to nozzles at the intake of the wind tunnel.
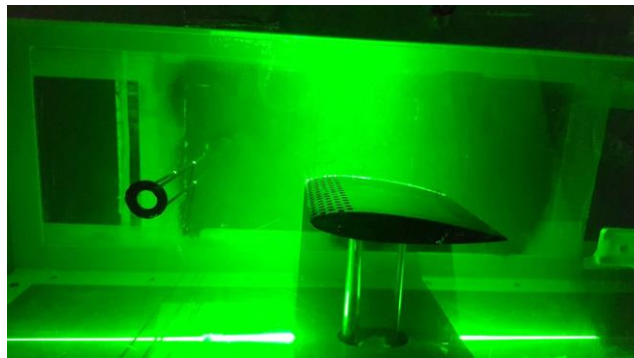

Fig. 4.4. Illuminated test section

A high-resolution CCD PIV camera (PIVCAM 10-30) with resolution of 1007 x 1017 pixels and interframe capability of $<\ 1\ \mu s$ was set up with its axis perpendicular to the laser sheet

17

for image acquisition. The CCD camera and the Nd:YAG lasers were connected to a workstation with an external programmable timing unit (Berkeley Nucleonics 'Pulse Generator'), which controlled the timing of the laser illumination and the image acquisition. LaVision DaVis software was used for control of the parameters. Instantaneous PIV velocity vectors were obtained by a frame to frame cross-correlation technique involving successive frames of patterns of particle images in multi-pass interrogation process from window size of 128×128 to 64×64 pixels. An effective overlap of 50% was employed. The time delay between the two frames was set between 50 μs and 450 μs depending on flow velocity to deliver adequate displacements within the flow velocity dynamic range.
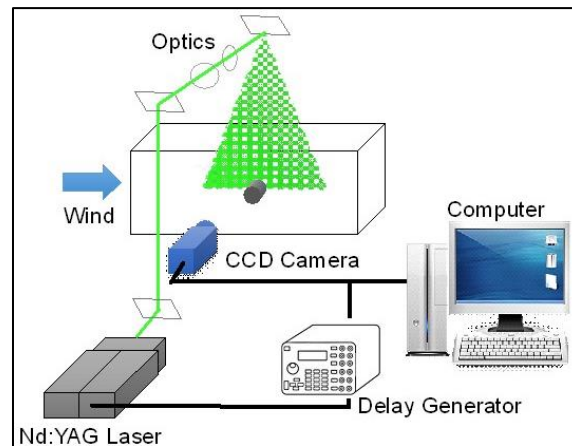

Fig. 4.5. PIV setup

4.2. Uncertainty

Experimental uncertainties in PIV can be due to various causes. Since PIV evaluates the change in distance over a known time interval of an individual seed particle the result is a velocity vector field. That field given by the equation;

$$u_{piv} = M \frac{\Delta s}{\Delta t}$$ (Eq. 4.1)

18

Where M is a magnification factor determined during camera calibration. If we express the percentage error in each value of the above equation as $\delta(\Delta s), \delta(\Delta t), and\ \delta(\Delta M)$ then the overall percentage error is calculated using the Kline-McClintock measurement uncertainty formula where;

$$\delta\left(u_{piv}\right) = \sqrt{\delta(M)^2 + \delta(\Delta s)^2 + \delta(\Delta t)^2} \qquad \text{(Eq. 4.2)}$$

This PIV study uses a two-dimensional image to capture the flow field where the magnification factor gives about 0.5% error. The timing unit used in this setup has an output resolution of 20ns meaning an error of 0.01%-0.04% of actual time difference. Lastly, the image pixel resolution is estimated at around 0.1 pixel which translates to about 1.23%-1.73% error in the image displacement. Combining the individual errors in the Kline-McClintock uncertainty equation the total error is found to be 1.32%-1.80%.

5. RESULTS AND DISCUSSION

5.1. Data Analysis

For each flow condition, a total of four plots were developed including instantaneous flow velocity contours/streamlines, average flow velocity contours, standard deviation contours and a profile of the u velocity behind the body. As noted previously, the velocity field is computed using the cross-correlation technique. The standard deviation contours are used to indicate a relative amount of turbulence; it will indicate the fluctuation of velocity at a given point in the flow. Standard deviation is given by the following equation;

$$\sigma = \sqrt{\frac{1}{n-1}\sum_i (x_i - \overline{x})^2} \qquad \text{(Eq. 5.1)}$$

Where the standard deviation (σ) of n images with x_i representing the pixel intensity of any pixel of image i and $\overline{x} = \frac{1}{n}\sum_{i=1}^{n} x_i$ representing the average [13] .

Next, streamlines are used to show the flow pattern. A streamline is defined as a line parallel to the velocity vector at any given point. This study will only make use of 2D streamlines but the full form of the velocity vector equations is $\vec{V}(x,y,z,t) = u\hat{\imath} + v\hat{\jmath} + w\hat{k}$. Where $d\vec{s} = dx\hat{\imath} + dy\hat{\jmath} + dz\hat{k}$ is an infinitesimally small vector along the streamline. Since $\vec{V}$ and $d\vec{s}$ are parallel, we can also write;

$$d\vec{s} \times \vec{V} = 0 \qquad \text{(Eq. 5.2)}$$

$$(wdy - vdz)\hat{\imath} + (udz - wdx)\hat{\jmath} + (vdx - udy)\hat{k} = 0 \qquad \text{(Eq. 5.3)}$$

Now setting the components of the cross product equal to zero we obtain three differential equations which describe the streamline. In the two-dimensional form where $dz = 0$ and $w = 0$ then we may write;

$$\frac{dy}{dx} = \frac{v}{u} \qquad \text{(Eq. 5.4)}$$

Once the velocity vector field has been obtained we can use this to then display the streamlines [13].

5.2. Circular Cylinder

The circular cylinder is a geometry which has been widely studied in the context of viscous flows. As a control verification, the PIV results obtained in this study for a solid circular cylinder in a rotating and non-rotating condition are presented here. The first case to be considered is that of the circular cylinder with no rotation at $Re = 83$. The instantaneous velocity contour/streamline plot in Fig. 5.1. shows the formation of a set of instantaneous vortices in the near wake region. At the next time step, the streamlines in Fig. 5.3. shows that the uppermost vortex has been shed but the lower one remains. This indicates that the flow is transitional and alternating between the forms of Fig. 2.6 b) and c).
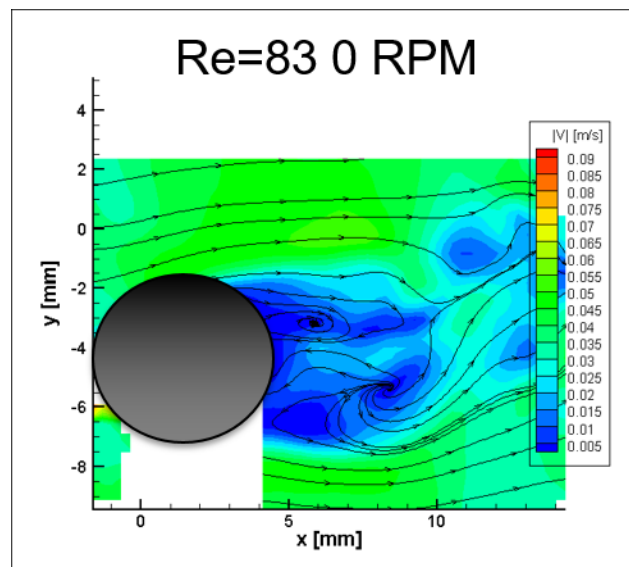

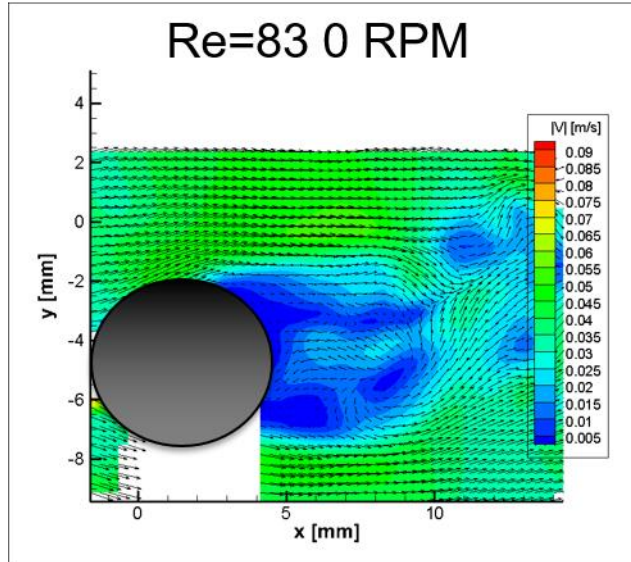Fig. 5.1. Instantaneous velocity contours/streamline

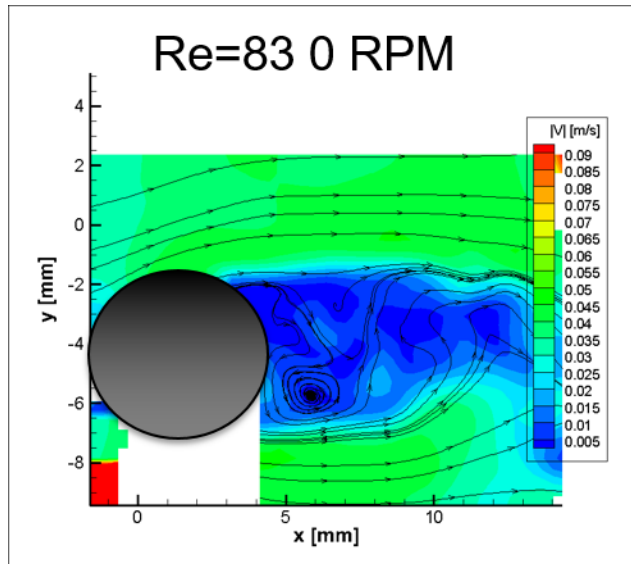Fig. 5.2. Instantaneous velocity contours/vectors

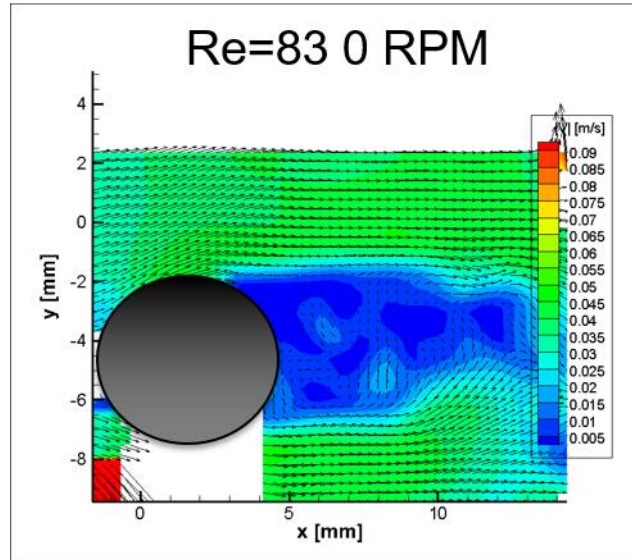

Fig. 5.3. Instantaneous velocity contours/streamlines

Fig. 5.4. Instantaneous velocity contours/vectors

The average velocity plot is useful to show the overall trends of the flow in a given time period. A series of one-hundred raw image sets were used to compute the average velocity plots in the present study. Fig. 5.5. shows a predictable flow behavior for the case of a circular cylinder at a low Reynolds number. Smooth transition from one contour to another and the absence of a steep gradient indicate that a stable vortex has not formed.
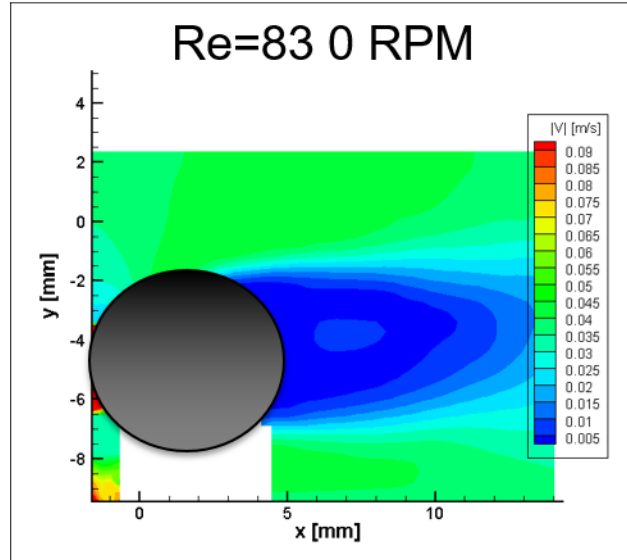
Fig. 5.5. Average velocity contours

As noted previously, a standard deviation plot will indicate local velocity fluctuation and therefore a relative amount of turbulence. The standard deviation plot for the non-rotating circular cylinder at $Re = 83$ in Fig. 5.6. reveals a low relative amount of turbulence in the near wake when compared to the non-rotating cylinder at $Re = 333$ in Fig. 5.7.
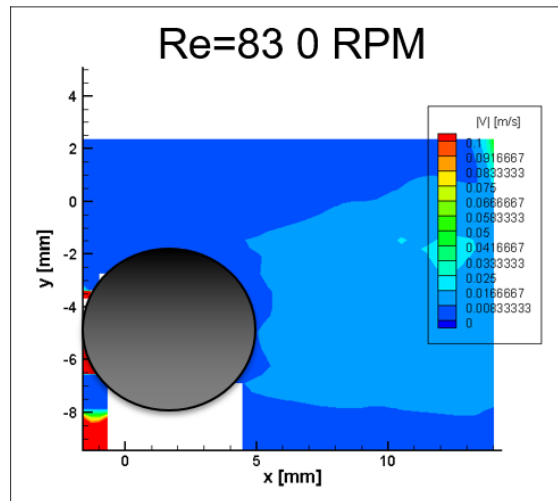

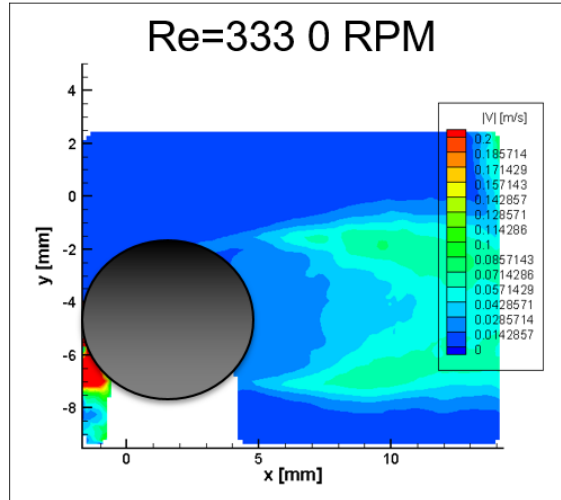Fig. 5.6. Standard deviation contours

24

Fig. 5.7. Standard deviation contours

Next, we will look at velocity profiles for three Reynolds numbers at three rotation speeds. The velocity profiles plot y location vs. average u velocity and are taken from $x = 7mm$ with respect to the calibrated camera frame. As with previous average velocity plots, a set of one-hundred images was used. The y vs. u velocity profile will help describe the formations in the near wake structure. In Fig. 5.8., which features the full cylinder profile at $Re = 83$, we see that for all rotation speeds there is a clear decrease in u velocity in the cylinder wake. At this Reynolds number the flow is laminar and transitions between velocity values are smooth. In Fig. 5.9. we begin to see a concave shape near the mid-point of the cylinder for all rotation speeds. This concave shape of the velocity profile could be due to one of two phenomena. The first explanation is that two large stable vortices have formed at the cylinder's trailing edge similar to Fig. 2.6. b). Since this flow is at $Re = 333$ a more likely scenario is that a Von Karman vortex street has formed and is causing a small increase in u velocity where the alternating vortexes transition as they are shed. This phenomenon would appear similar to the rendering in Fig. 2.6. c). Lastly, looking at the turbulent flow at $Re = 28796$ in Fig. 5.10. we see the concave shape washed out similar to the flow pattern seen in Fig. 2.6. d) and e).
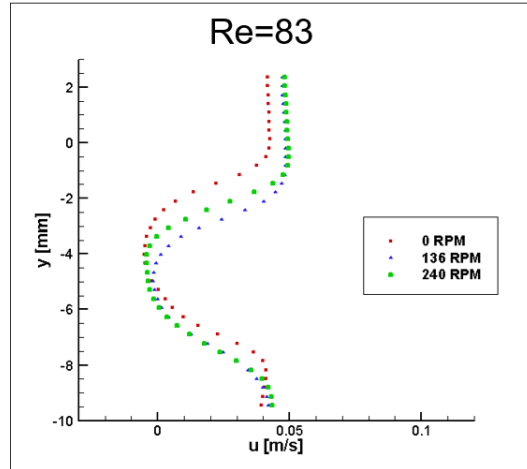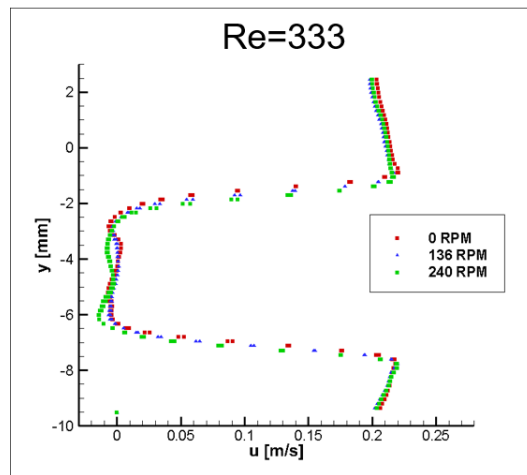
25

Fig. 5.8. u-Velocity profiles for $Re = 83$

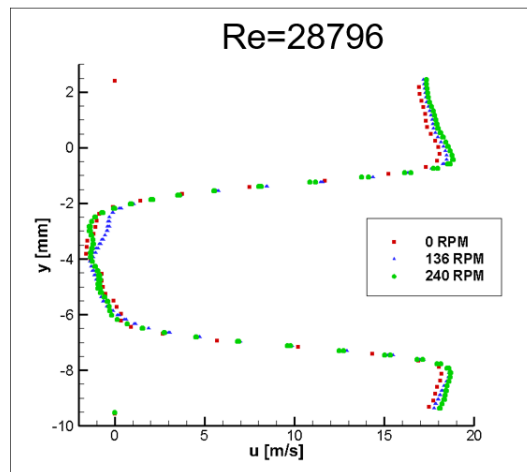Fig. 5.9. u-Velocity profiles for $Re = 333$

Fig. 5.10. u-Velocity profiles for $Re = 28796$

5.3. Sliced Cylinder

The sliced cylinder is a cylinder profile having horizontal and vertical slits of width $d/3$. When the cylinder is in a stationary condition it may be placed in either an open or closed orientation. The open orientation eliminates leading and trailing edge stagnation points by offering a direct fluid flow path through the cylinder. The closed orientation removes the direct path and again introduces leading and trailing edge stagnation points. By inspection of the velocity profiles in Fig. 5.11. there is a clear jet structure formed in the wake of the sliced cylinder in an open orientation. Beginning at $y = -2$ and continuing until $y = -4$ there is a sharp increase and then decrease of the u velocity. Conversely, for the closed orientation the velocity profile resembles that of the spinning sliced cylinder or the full cylinder.
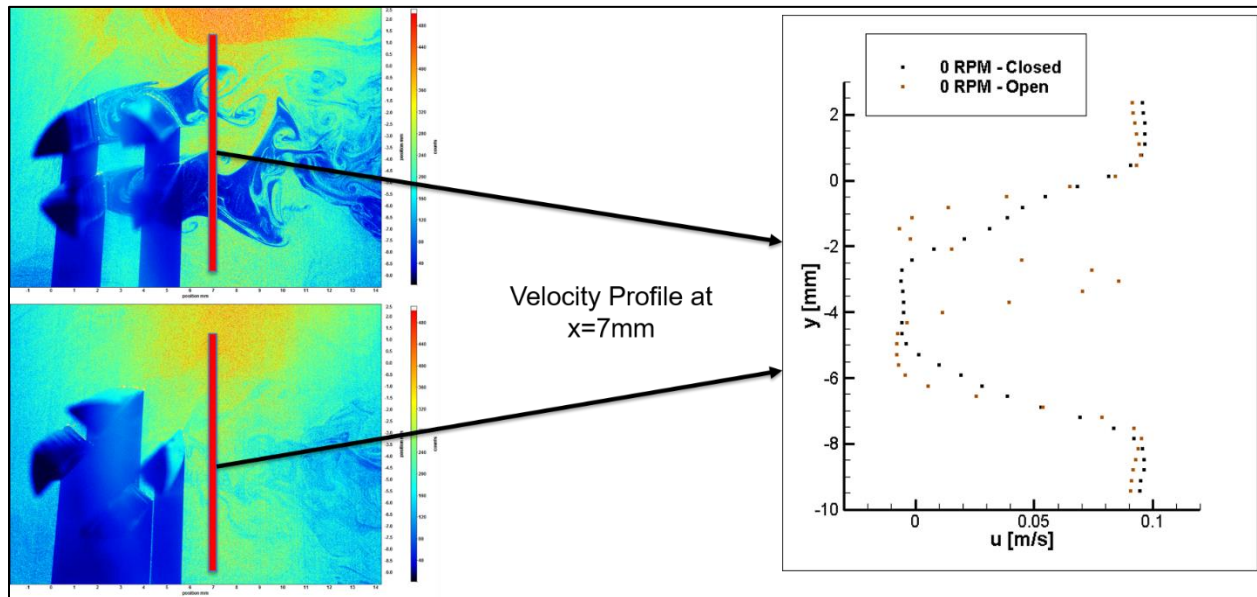

Fig. 5.11. Raw images of open/closed orientation and corresponding velocity profiles at $Re = 166$

Next, we will turn our attention to the sliced cylinder in a rotating condition. Compared to the static condition of the sliced cylinder, the rotating sliced cylinder should provide much more

turbulent mixing in the wake structures. By inspection of the instantaneous velocity and streamline plot we immediately notice that the streamlines are directed downward into the free stream below the rotating cylinder. The instantaneous velocity plot also shows an area of low velocity magnitude on the upper right corner of the rotating cylinder. This phenomenon is also apparent in the average velocity plot and u velocity profile. A small velocity magnitude coupled with a dip in the u velocity component indicates that stagnation point has formed in this area. Compared to the case of a rotating circular cylinder, where stagnation points move downward assuming clockwise rotation, the sliced cylinder shows the stagnation point moving upward.
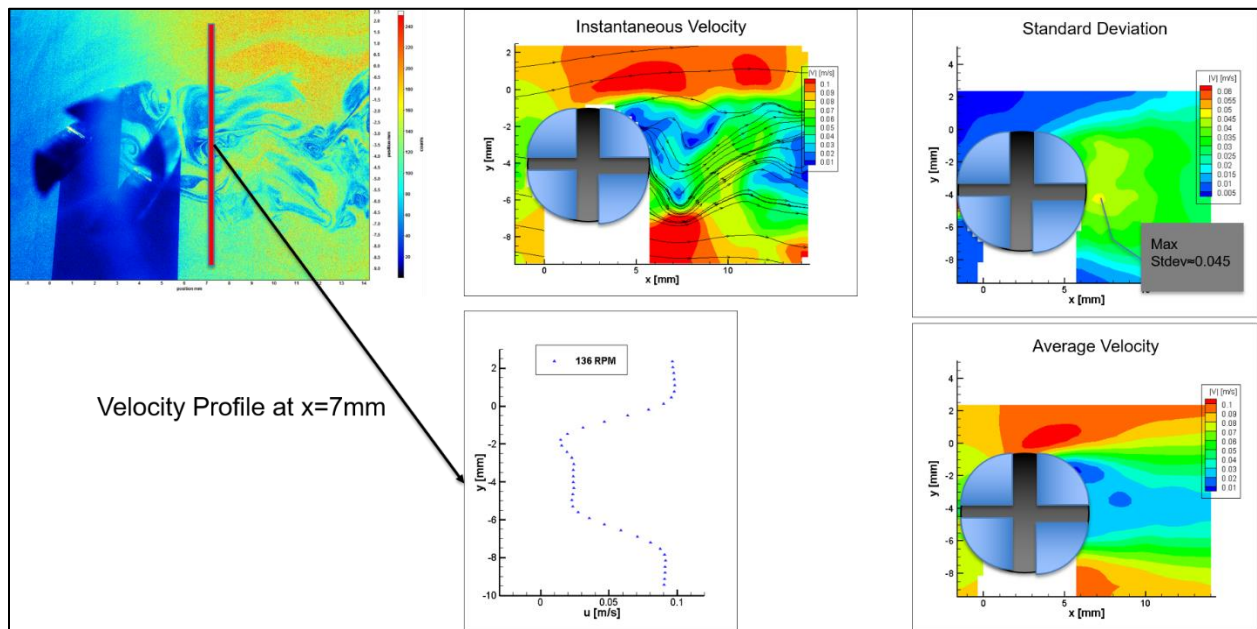

Fig. 5.12. All plots generated for sliced cylinder at $Re = 166$ and rotation speed of $136\ RPM$

5.4. Three Cylinder Setup

In this section, we discuss the effect of the cylinder apparatus rotation on near-wake structures. Figs. 5.13. through 5.15. compare standard deviation plots for the three-cylinder apparatus all at $Re = 645$ with varying rotation speeds. By inspection of the non-rotating case

three branches of higher standard deviation can be seen emanating from the three-cylinder setup in Fig. 5.13. These branches indicate the y position of each of the three small cylinders. For the rest of the plot, standard deviation values transition smoothly and predictably from one contour to another. Looking at the next case where the cylinder apparatus is set in motion at 136 RPM in Fig. 5.14. we see that the branches are washed out in the very near wake and a smooth jet of higher standard deviation is formed. As the distance from the cylinder apparatus is increased, the branch structure begins to form again indicating a decrease in the formation of turbulent vortexes. When rotation is increased to 240 RPM in Fig. 5.15. we see the washing out effect continue in the near wake and the area of higher standard deviation become larger.
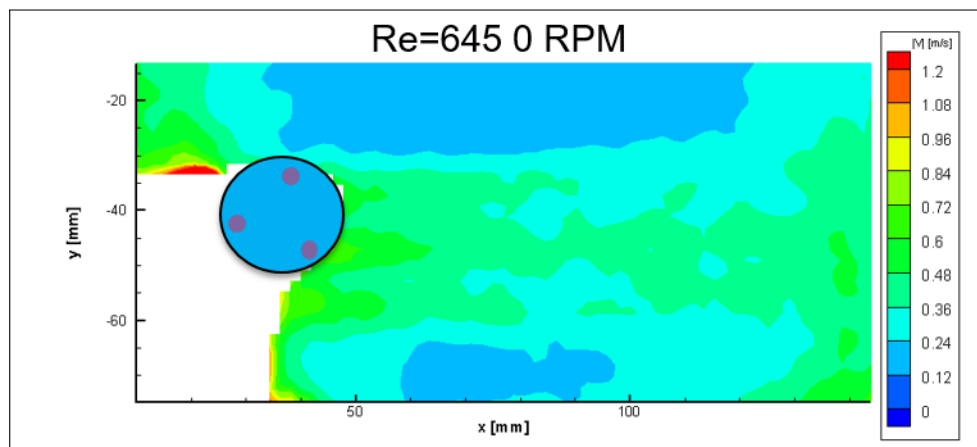

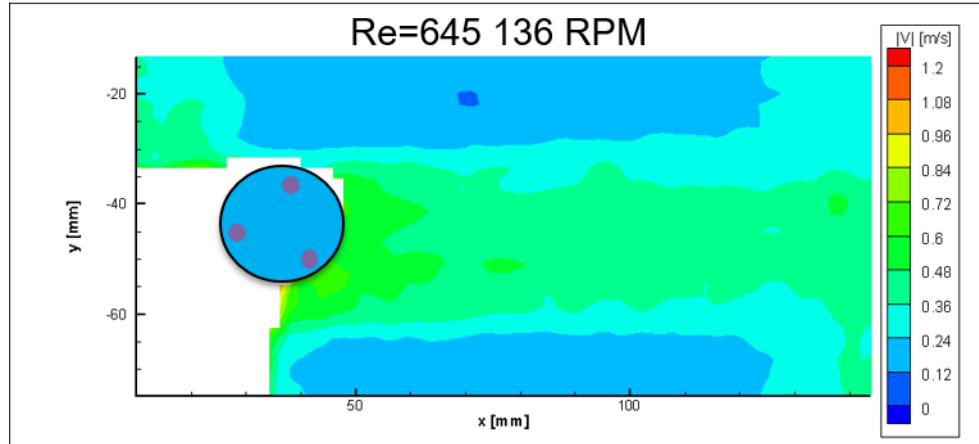Fig. 5.13. Standard deviation contours for $Re = 645$ at $0 \ RPM$

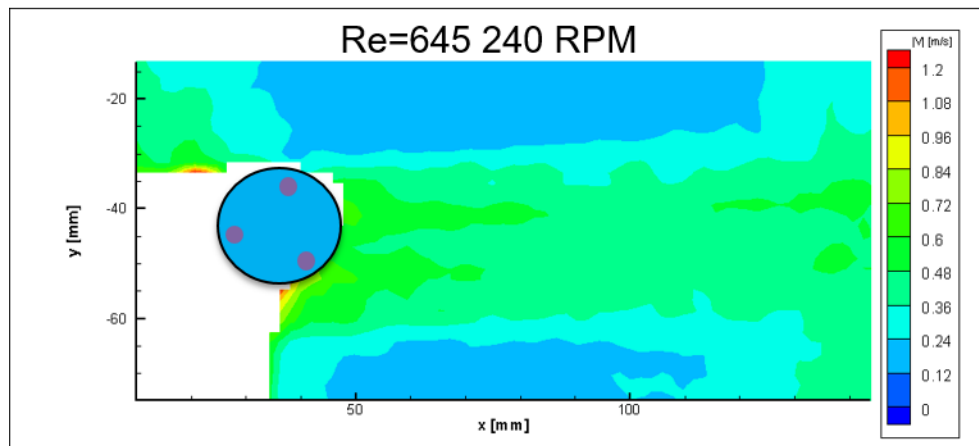Fig. 5.14. Standard deviation contours for $Re = 645$ at $136\ RPM$

Fig. 5.15. Standard deviation contours for $Re = 645$ at $240\ RPM$

Next, we will we will look at how rotation of the three-cylinder arrangement affects velocity profiles. Looking at the velocity profile for the static case in Fig. 5.16. the location of the three cylinders will be detected where the u velocity makes a sharp dip near $y = -35mm$ and a shallower dip at $y = -55mm$. In this case, since the cylinders are oriented as shown in the raw image, Fig. 5.16, the sharper dip is seen where the top two cylinders are in line. Looking at the plots for cylinder rotation at 136 and 240 RPM a smoother profile is seen.
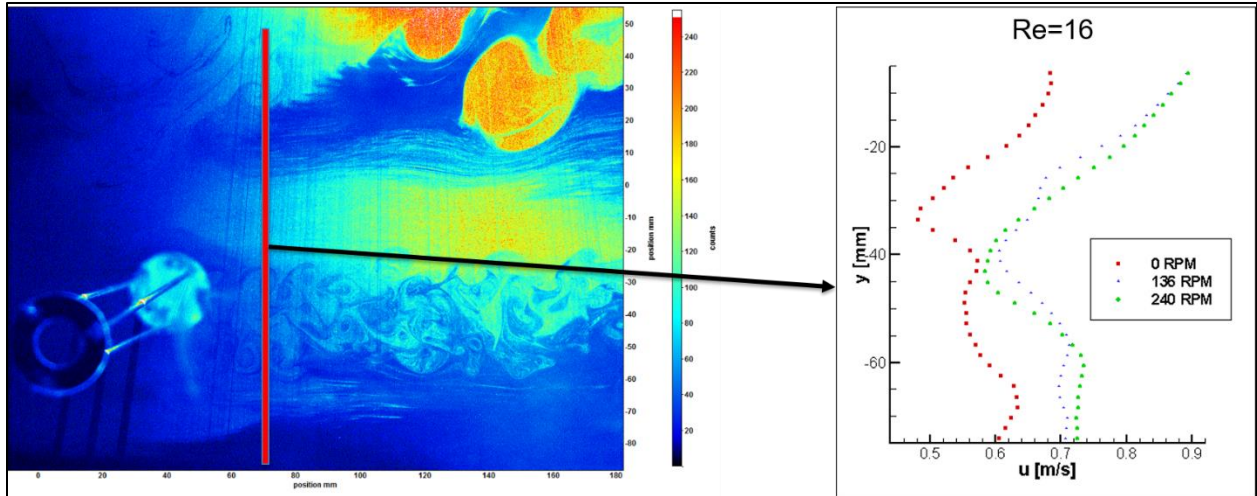
Fig. 5.16. Raw image and velocity profiles at $Re = 16$

Next, we will observe how rotation speed affects instantaneous velocity contours and streamline plots for the three-cylinder arrangement at $Re = 16$. Plots of instantaneous vorticity in the z direction are also included. Comparing the instantaneous velocity plots, we see that there is a small area of low velocity magnitude on the bottom, trailing edge of the cylinder arrangement rotating at 240 RPM in Fig. 5.19. This feature is not present however at the lower rotation speed of 136 RPM as shown in Fig. 5.17. The area of low velocity magnitude is likely caused by the increased rotation speed causing a bubble of fluid with low kinetic energy to form in this area. The exact orientation of the cylinder arrangement at the instant in which this data was captured could also be an influencing factor. Vorticity plots for both rotation speeds in Fig. 5.18. and Fig. 5.20. show intermittent staggered areas of high vorticity.
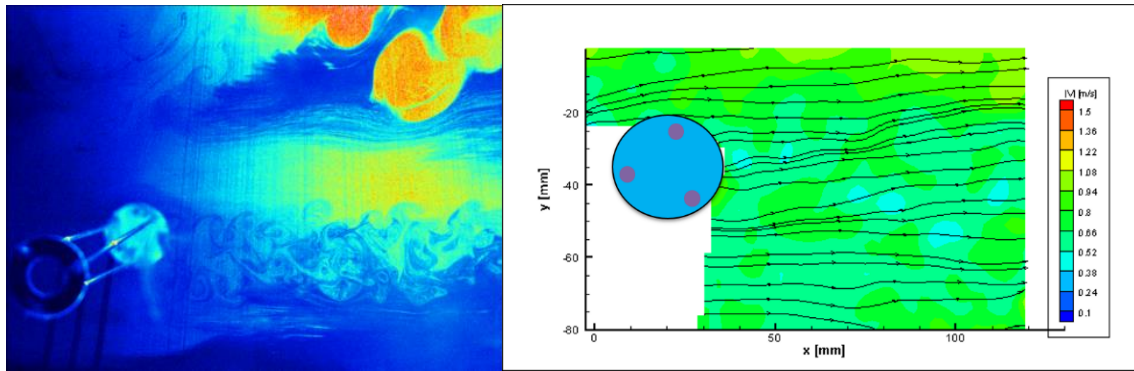
Fig. 5.17. Raw image and instantaneous velocity contour/streamline plot at $Re = 16$ and cylinder rotation 136 RPM
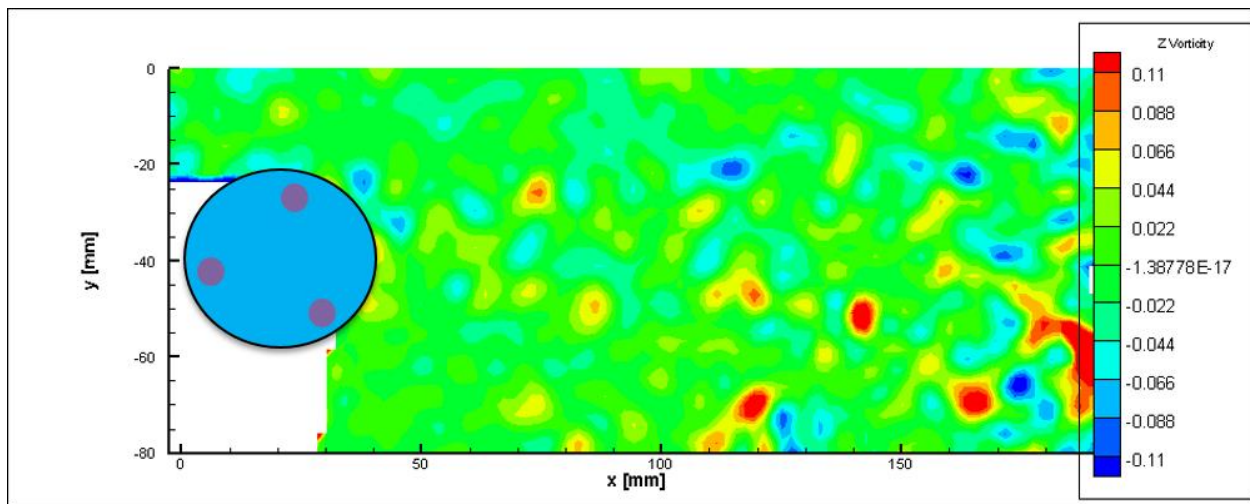

Fig. 5.18. Vorticity contours at $Re = 16$ and cylinder rotation at 136 RPM
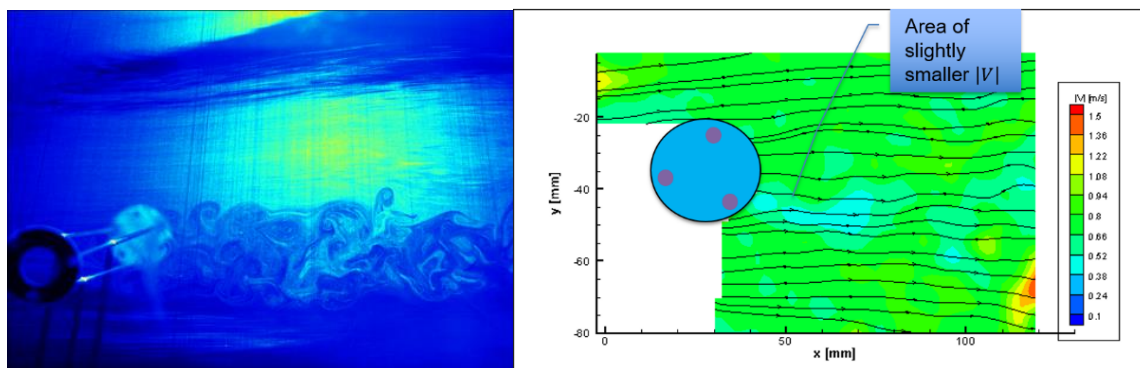

Fig. 5.19. Raw image and instantaneous velocity contour/streamline plot at $Re = 16$ and cylinder rotation 240 RPM

32
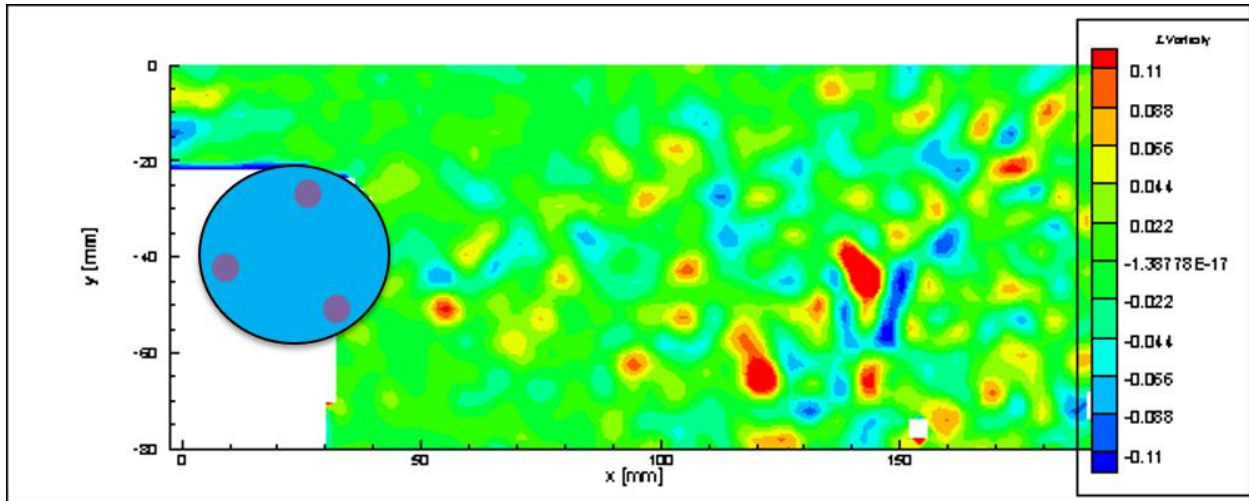
Fig. 5.20. Instantaneous vorticity contours at $Re = 16$ and cylinder rotation at 240 RPM

5.4.1. Measuring Turbulence in Wake of Three Cylinder Setup

A hot wire anemometer was another method used to measure turbulence created by the three-cylinder system. The wire, located downstream of the cylinder system as seen in Fig. 5.21., was used to measure turbulence levels and track flow frequencies which can be related to Strouhal number.
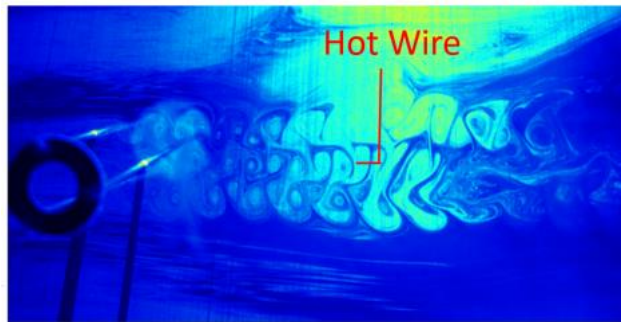
Fig. 5.21. Hot wire anemometer location in the wake of three-cylinder system

In the free stream, the hot wire anemometer yielded less than 5% turbulence. When placed behind the three-cylinder system, the time series revealed an interesting mix of frequencies for various speeds and rotations.

Fig. 5.22. displays hot wire traces mixed with a carrier (heterodyned) to highlight turbulence patterns. Periodic motions and increase in randomness/turbulence can be appreciated for various flow speeds from the hot wire time series samples shown.
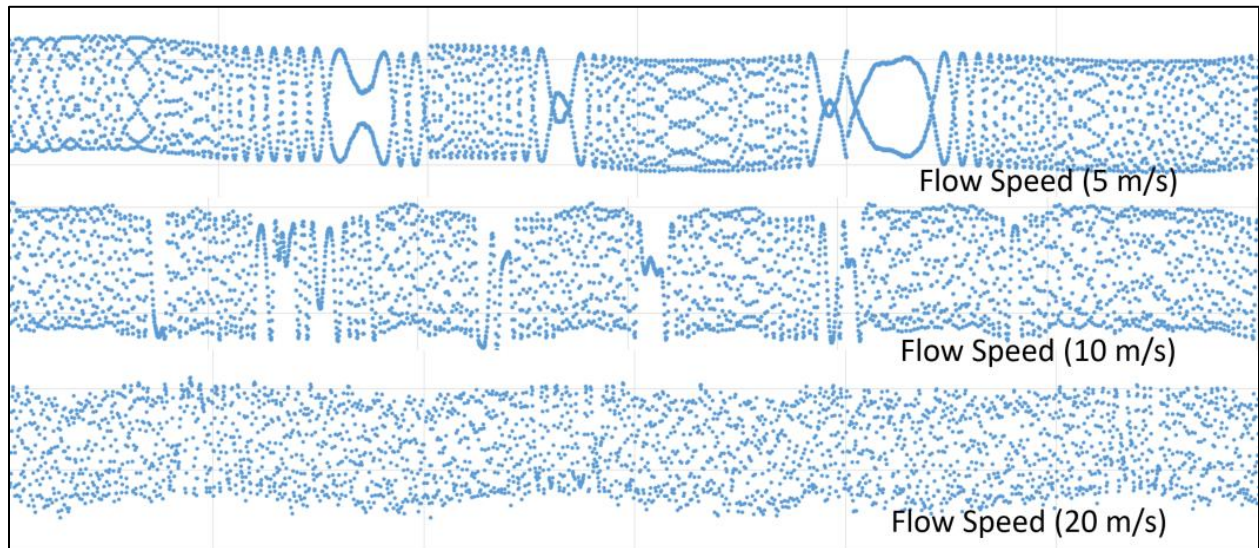
Fig. 5.22. Hot wire traces mixed with a carrier for various flow speeds. Each plot shown was taken at 2.5 kHz for a total of 1 second sample time.

Fig. 5.23 shows samples of frequency spectra without filtering. It is noted that each condition has distinctive frequency peaks and that some conditions appear to annihilate large frequencies. This may indicate that dynamic interaction of the wake structures produces direct mixing into small scale turbulence.
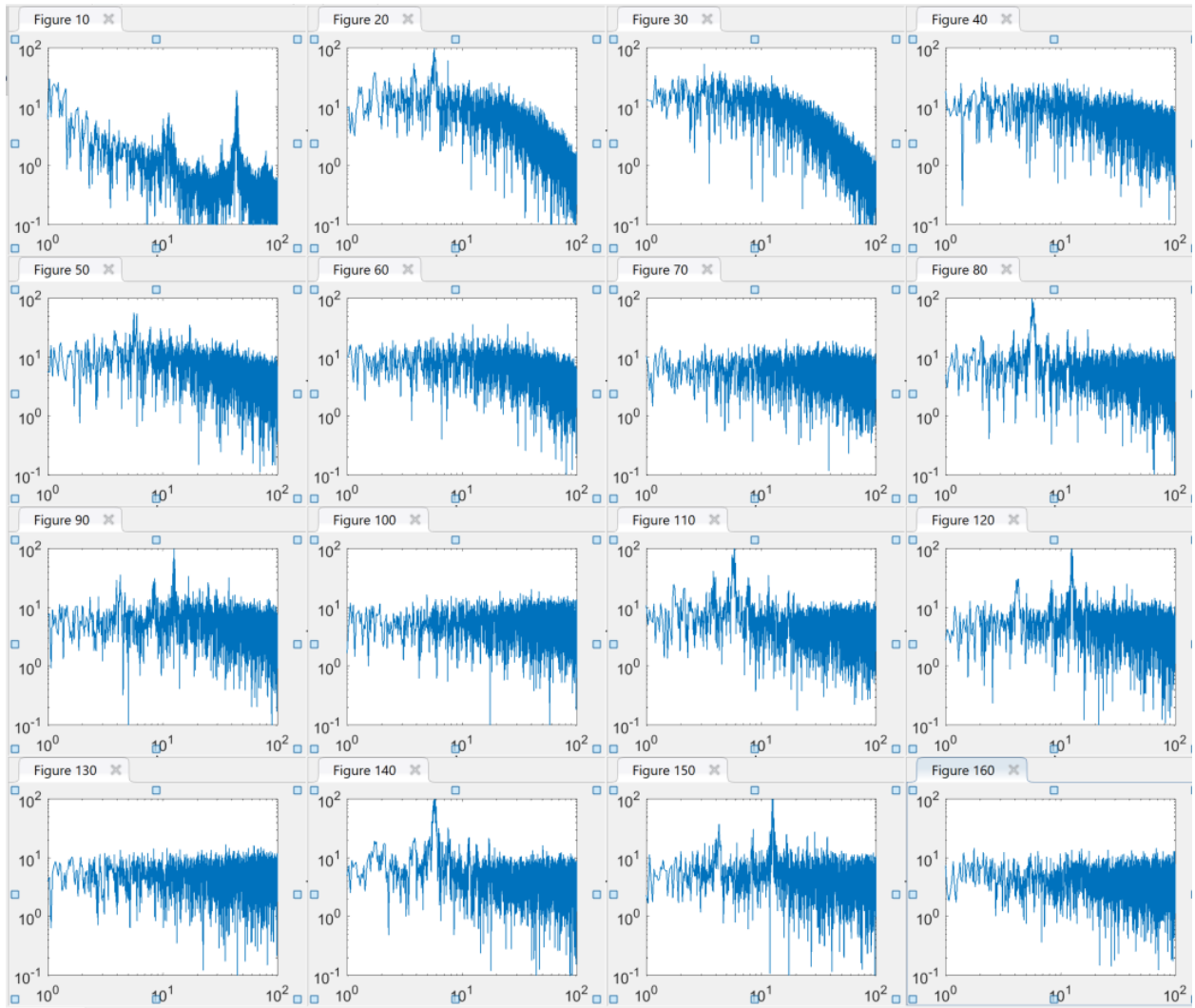
Fig. 5.23. Frequency spectra without filtering for hot wire anemometer data. Flow conditions for each figure are cross-referenced with Table 5.1 below.

Table 5.1. Flow conditions for data in Fig. 5.23.

Free Stream (m/s)	Rotation 0 RPM	Rotation 136 RPM	Rotation 240 RPM
0.5	Figure 10	Figure 20	Figure 30
1	Figure 40	Figure 50	Figure 60
4	Figure 70	Figure 80	Figure 90
6	Figure 100	Figure 110	Figure 120
8	Figure 130	Figure 140	Figure 150
10	Figure 160	N/A	N/A

5.5. Highly Turbulent Flow Over Dimpled Airfoil

The next phase of the present study deals highly turbulent flow over the symmetric, dimpled airfoil seen in Fig. 5.24. The dimpled airfoil is created from a NACA 0015 profile and the turbulence is artificially generated by rotation of the three-cylinder apparatus. Rotation speeds of 0, 136 and 240 were again used for each case. The experimental methodology remains the same for this setup, however, a second camera was added to capture the entire width of the test section. The PIV technique remains two-dimensional and the vector fields produced by both cameras were stitched together during post processing.
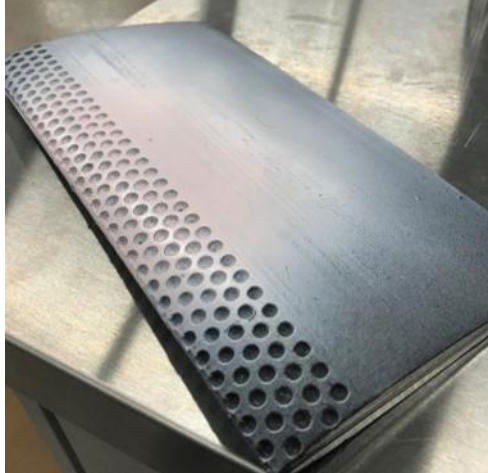
Fig. 5.24. Dimpled Airfoil

Turning our attention to the average velocity magnitude contour plot for the dimpled airfoil at a low angle of attack we show that the flow remains attached to the airfoil along the entire chord length for both high and low Reynolds numbers. Upon inspection of some instantaneous velocity plots the flow appears to momentarily detach from the airfoil surface. The exact cause of the momentary flow detachment is not known. Because of the swirling action caused by the dimpled surface further analysis using a volume tomographic study would be required to uncover the underlying mechanisms behind momentary flow detachment. Another feature of note in Fig. 5.25 is the higher velocity magnitude seen stretching across the entire dimpled surface.
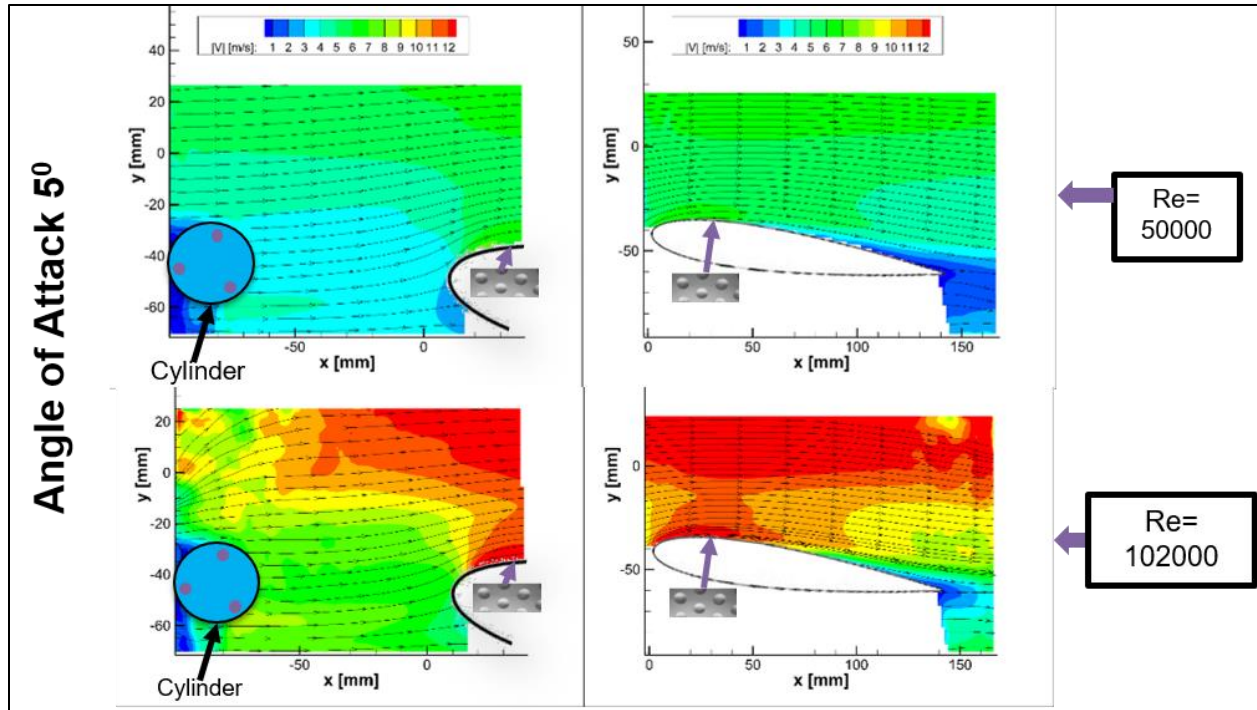
Fig. 5.25. Average velocity contours and streamlines for dimpled airfoil at low angle of attack

Now, we will turn our attention to the same flow conditions where the airfoil's angle of attack has been increased to 15°. In Fig. 5.26 we see the flow has detached near the leading edge and a recirculation bubble has formed in the wake. When the Reynolds number is increased, the recirculation bubble collapses and becomes less defined. Looking at some instantaneous velocity plots for this condition, we see that there is momentary flow reattachment at some time steps as seen in Fig. 5.27.
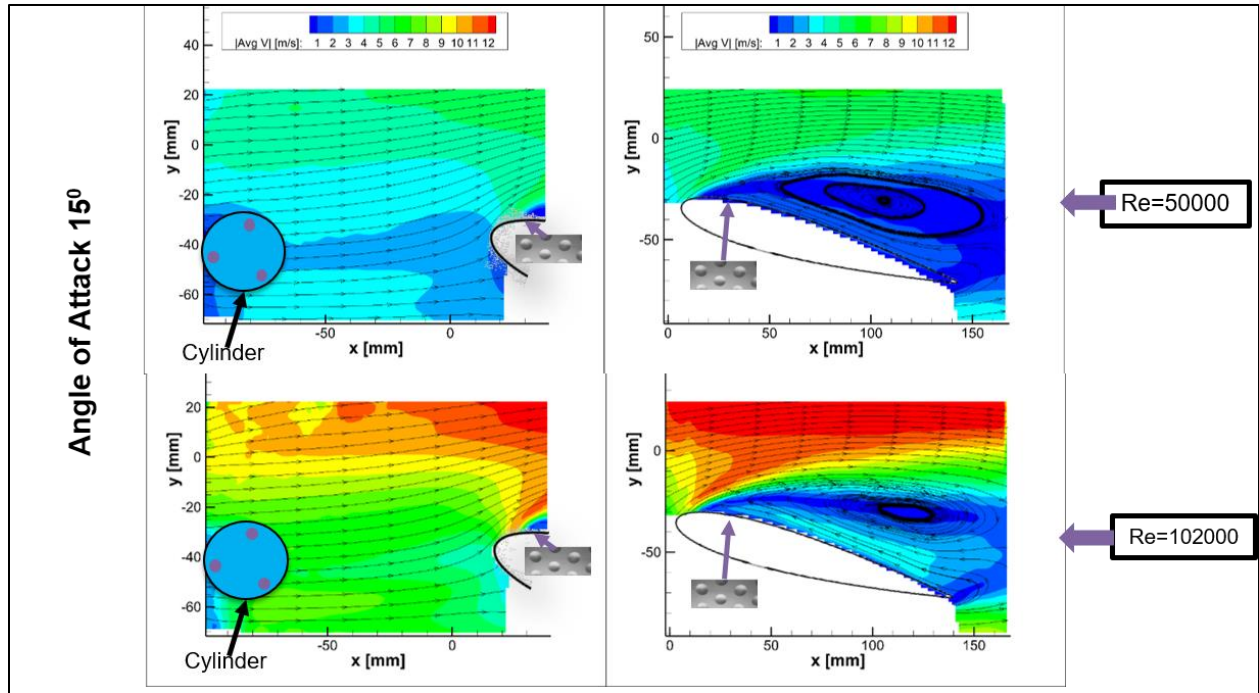
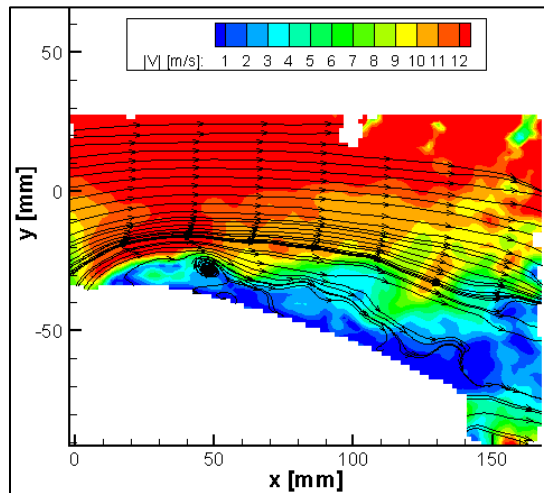Fig. 5.26. Average velocity contours and streamlines for dimpled airfoil at high angle of attack

Fig. 5.27. Instantaneous reattachment of flow over dimpled airfoil for AOA 15° and $Re =$ 50000

6. CONCLUSION AND FUTURE WORKS

It has been shown in this study that the circular cylinder, sliced cylinder, and three-cylinder arrangement have differing effects on the velocity fields and on the relative amounts of turbulence they generate. One key conclusion that can be drawn from this study is that rotation of the sliced cylinder shows a significant redirection of the instantaneous streamlines near the trailing edge. Streamline redirection is caused by rotation of the cylinder. This can be seen in its instantaneous velocity plots and the locations of high and low velocity magnitude in the average velocity plots. Next, it has been shown that higher Reynolds numbers likely eliminate the alternate vortex shedding in the wake of the circular cylinder for all rotation speeds. This is shown by the washout of the concave shape that formed in the velocity profiles for the circular cylinder at $Re = 333$. Lastly, it was found that turbulence in the wake of the three-cylinder apparatus steadily increases as rotation speed goes from $0\ RPM$ to $240\ RPM$.

To more accurately observe the mechanisms at work in this study, a 3-D volume tomographic study is required. One problem with 2-D PIV is that since the laser beam has been shaped into a 1mm thick sheet, the particles may move laterally in and out of the laser sheet. This causes error in the velocity field computation. The lateral movement of particles would be most pronounced in the case of the dimpled airfoil because of the swirling going on inside each dimple. To expand upon the present study, more cylinder geometries could be testing including increasing the diameter of the cylinders, adding another cylinder to the three-cylinder setup, or altering the profile of the sliced cylinder. Rotation speed could also be increased past the $240\ RPM$ limit to observe its effects.

REFERENCES

[1] M.M. Alam and J.P. Meyer, "Two interacting cylinders in cross flow," *Physical Review* Vol. 84 2011 [Accessed February 1, 2018]

[2] S. Aradag "Unsteady Turbulent Vortex Structure Downstream of a Three Dimensional Cylinder." *Thermal Science and Technology*. Available: Elsevier, [Accessed February 1, 2018]

[3] C.D Cantwell and D. Barkley. "Computational study of subcritical response in flow past a circular cylinder," *Physical Review* E 82, 026315. 2010 Available: Elsevier, [Accessed February 1, 2018]

[4] S. Dennis and C.R. Chang, 1970. "Numerical solutions for steady flow past a circular cylinder at Reynolds numbers up to 100," *Journal of Fluid Mechanics* 42, 471–489. Available: Elsevier, [Accessed February 2, 2018]

[5] S. Dong, G.E. Karniadakis, A. Ekmecki, and D. Rockwell, "A combined Direct Numerical Simulation-Particle Image Velocimetry Study of the Turbulent Near Wake," *Journal of Fluid Mechanics*, Vol 569, pp. 185-207 2006 Available: Elsevier, [Accessed February 10, 2018]

[6] F. Durand, *Aerodynamic Theory*. Dover Publications, 1963.

[7] Engineering ToolBox, *Laminar, Transitional or Turbulent Flow*. (2004). [online] Available at: https://www.engineeringtoolbox.com/laminar-transitional-turbulent-flow-d_577.html [Accessed March, 23 2018].

[8] D. Gao, W. Chen, H. Li, and H. Hu, "Flow Around a Circular Cylinder with a Slit," *Experimental Thermal and Fluid Science*, Vol. 82, pp. 287-301, 2016 Available: Elsevier, [Accessed February 15, 2018]

[9] K. Hourigan, M.C. Thompson, G.J. Sheard, K Ryan, J.S. Leontini, and S.A. Johnson, "Low Reynolds Number Instabilities and Transitions in Bluff Body Wakes." *Journal of Physics*, vol. 64, no. 60, June 2007. *IOP Science*. Available: Elsevier, [Accessed February 15, 2018]

[10] T. Igarashi,. "Characteristics of the flow around two circular cylinders arranged in tandem,". *Bulletin of JSME* 24, 323–331. 1981 Available: Elsevier, [Accessed February 15, 2018]

[11] N. Kim, H. Kim, and H. Park, "An Experimental Study on the Effects of Rough Hydrophobic Surfaces on the Flow Around a Circular Cylinder," *Physics of Fluids*, Vol. 27 pp, 1-23 2015 Available: Elsevier, [Accessed February 10, 2018]

[12] B. Kumar, S. Mittal,. "Effect of blockage on critical parameters for flow past a circular cylinder*," International Journal for Numerical Method in Fluids* 50, 987–1001. 2006 Available: Elsevier, [Accessed February 11, 2018]

[13] LaVision GmbH (2008) Davis 7.2: Product Manual Gottingen, Germany

[14] K. Lee, and K.S. Yang, "Flow patterns past two circular cylinders in proximity," *Computers and Fluids* 38, 778–788. 2009 Available: Elsevier, [Accessed February 16, 2018]

[15] H. Lim, and S. Lee, "Flow Control of Circular Cylinders with Longitudinal Grooved Surfaces," *AIAA Journal*, Vol. 40, No:10, October 2002 Available: Elsevier, [Accessed February 16, 2018]

[16] L. Lu, M. Liu, B. Teng, Z. Cui, G. Tang, M. Zhao, L. Cheng, "Numerical Investigation of Fluid Flow Past Circular Cylinder with Multiple Control Rods at Low Reynolds Number." *Journal of Fluids and Structures*, vol. 48, no. 48, 13 Apr. 2014, pp. 235–259. Available: Elsevier, [Accessed February 10, 2018]

[17] J. C. Lin, J. Towfighi, and D. Rockwell, "Instantaneous Structure of a Near Wake of a Cylinder: On the Effect of Reynolds Number," J. *Fluids Struct.,* Vol. 9, pp. 409-418, 1995 Available: Elsevier, [Accessed February 10, 2018]

[18] X. Ma, G.S. Karamanos, and G.E. Karniadakis, "Dynamics and Low-Dimensionality of a Turbulent Near Wake," *Journal of Fluid Mechanics*, Vol. 410, pp. 29-65, 2000 Available: Elsevier, [Accessed February 11, 2018]

[19] J. R. Meneghini, F. Saltara,. "Numerical simulation of flow interference between two circular cylinders in tandem and side-by-side arrangements" *Journal of Fluids and Structures* 15, 327–350. 2001 Available: Elsevier, [Accessed February 21, 2018]

[20] C. Norberg, "Flow around a circular cylinder: aspects of fluctuating lift*" Journal of Fluids and Structures* 15, 459–469. 2001 Available: Elsevier, [Accessed February 11, 2018]

[21] V. Oruc, H. Akilli, and B. Sahin, "PIV Measurements on the Passive Control of Flow Past a Circular Cylinder," *Experimental Thermal and Fluid Science*, Vol. 70 pp. 283-291, 2016 Available: Elsevier, [Accessed February 11, 2018]

[22] I. Peschard, and P. LeGal, "Coupled wakes of cylinders," *Physical Review Letters* 77,3122–3125. 1996 Available: Elsevier, [Accessed February 11, 2018]

[23] H. Schlichting, *Boundary-Layer Theory*. 6th ed., vol. 1 of 4, McGraw Hill Book Company, 1968.

[24] S. Sen, S. Mittal, and G. Biswas, "Steady separated flow past a circular cylinder at low Reynolds numbers," *Journal of Fluid Mechanics* 620, 89–119. 2009 Available: Elsevier, [Accessed February 12, 2018]

[25] B. Sharman, F.S. Lien, L. Davidson, and C. Norberg, "Numerical predictions of low Reynolds number flows over two tandem circular cylinders," *International Journal for Numerical Method in Fluids* 47, 423–447. 2005 Available: Elsevier, [Accessed February 11, 2018]

[26] S. Singha, K.P. Sinhamaahapatra, "High-resolution numerical simulation of low Reynolds number incompressible flow about two cylinders in tandem" *Journal of Fluids Engineering* 132. (011101-1). 2010. Available: Elsevier, [Accessed February 21, 2018]

[27] D. Sumner, S.J. Price, and M.P. Païdoussis, "Flow-pattern identification for two staggered circular cylinder in cross-flow" *Journal of Fluid Mechanics*, 263–303. 2000 Available: Elsevier, [Accessed February 19, 2018]

[28] A. Stolt, J. Estevadeordal, Y. Zhang, J. Krech "A tomographic PIV and TSP study of leading-edge structures on stall behaviors of NACA 0015

[29] Teapeat. "Reynolds Behaviors." *Wikimedia Commons*, Wikimedia, 22 Dec. 2012, commons.wikimedia.org.

[30] A. Vakil, and S.I. Green, "Two-dimensional side-by-side circular cylinders at moderate Reynolds numbers," *Computers and Fluids* 51, 136–144. 2011 Available: Elsevier, [Accessed February 19, 2018]

[31] C. H. Williamson, "Vortex dynamics in the cylinder wake," *Annual Review of Fluid Mechanics* 28, 477–539. 1996 Available: Elsevier, [Accessed February 19, 2018]

[32] S. Yagmur, S. Dogan, M. Aksoy, I. Goktepeli, and M. Ozgoren, "Comparison of Flow Characteristics Around an Equilateral Triangular Cylinder via PIV and Large Eddy Simulation Methods*," Flow Measurement and Instrumentation*, Vol. 55, pp. 23-36, 2017 Available: Elsevier, [Accessed February 19, 2018]

[33] M. Zdravkovich, "Smoke observations of the wake of a group of three cylinders at low Reynolds number," *Journal of Fluid Mechanics* 32, 339–351. 1968 Available: Elsevier, [Accessed February 19, 2018]

[34] M. Zradkovich, "Conceptual Overview of Laminar and Turbulent Flows Past Smooth and Rough Circular Cylinders," *Journal of Wind Engineering Indust. Aero*, Vol. 33, pp. 53-62, 1990 Available: Elsevier, [Accessed February 19, 2018]